# Analysis of formability of advanced high strength steel sheets with phenomenologically based failure criteria with separate treatment of instability, shear and normal fracture

Isik, K.[a], Soyarslan, C. [a], Richter, H. [b], Tekkaya, A.E. [a]

[a] Institute of Forming Technology and Lightweight Construction
Technical University of Dortmund, 44227, Dortmund, Germany
[b] ThyssenKrupp Steel Europe AG, Duisburg, Germany

## Abstract

*Despite their wide application in sheet metal forming analysis, Forming Limit Diagrams cannot supply reliable results for the cases involving non-proportional strain paths or material classes with reduced ductility such as advanced high strength steels (AHSS). Fracture criteria appear as complimentary tools for assessment of formability in these cases. CrachFEM, as an advanced failure model, merges an instability criterion that includes strain hardening and yield loci effects with fracture criteria which monitor damage accumulation for ductile normal fracture and ductile shear fracture separately where stress triaxiality ratio and maximum shear stress dependence are taken into account, respectively. In the present study, rectangular deep drawing of two AHSS classes is studied both experimentally and numerically. Blanks with different rolling directions and blank orientations with respect to the punch are taken into account. Simulations are conducted using CrachFEM failure model and LS-DYNA where texture of the sheet due to rolling is modeled with Hill'48 type anisotropic yield locus. Experimental studies reveal that the failure occurs mainly due to instability with necking whereas in-plane shear stress state in drawing zone seems to be insufficient to create shear fracture. Numerical results show not only the predictive capability of CrachFEM but also regarding weaknesses which needs improvement for better predictions.*

**Keywords:** CrachFEM failure model, Anisotropy, Deep drawing, AHSS.

## 1. Introduction

Use of AHSS is rising in manufacturing industry due to simultaneously achieved component properties such as low weight and high strength. Formability of metal sheets is generally limited by localized necking [Hosford and Caddell, 1993] where forming limit curves (FLCs) are beneficial instruments in obtaining these limits with respect to the onset of local instability by tension. Despite their wide usage and benefits, FLCs fall short in determination of the formability for the cases involving nonlinear strain paths and cases where fracture happens before the onset of necking (e.g. ductile normal fracture of bending of materials with reduced ductility and ductile shear fracture under low and negative triaxiality ratios). This gap can be bridged by devising accumulative damage models which are useful not only for forming simulations but also for the determination of crashworthiness. In this study, we present formability analysis of complex phase (CP) steels, which consist of a complex bainitic basic structure with smaller amounts of martensite and perlite, with both experimental and numerical aspects.

The experimental studies involve deep drawing tests conducted in facilities of ThyssenKrupp Steel Europe AG for two steel grades. These studies intend not only to observe the effect of various process parameters on the blank formability but also to produce a large validation space for numerical studies. For this purpose, tests are conducted for different blank orientations with respect to the punch and different rolling directions with respect to the blank edge and different blank-holder pressures.

Numerical studies are conducted using LS-DYNA in conjunction with the material model MF GenYld+CrachFEM. The motivation behind selection of CrachFEM for failure prediction is twofold. Firstly, CrachFEM gives account for the failure modes due to necking (implying non-linear path effects) which is a common failure mode in many sheet metal forming operations. Secondly, this failure model monitors ductile normal and shear fracture risks separately, where susceptibility of the AHSS to the shear fracture is already noted in the literature, [Li et al., 2010]. As a consequence, CrachFEM presents itself as an ideal failure module, which embraces an instability criterion and two fracture criteria, for sheet metal formability. The simulations are conducted for all experimental scenarios and the results are discussed in detail on the basis of the experimental results.

This paper has the following outline. CrachFEM failure model is summarized in Section 2. The experimental studies and numerical investigations are presented in Section 3. Finally, the conclusions are drawn in Section 4.

## 2. The CrachFEM Failure Model

CrachFEM failure module investigates crack initiation considering three possible failure mechanisms separately. These failure mechanisms are:

- Local instability by tension
- Ductile normal fracture due to micro-void nucleation, growth and coalescence
- Ductile shear fracture due to shear band localization

Local instability criterion in CrachFEM is originated from well-known Marciniak and Kuczynski model, [Marciniak and Kuczynski, 1967], where the tensile instability is provoked by an initial imperfection. While retaining the main structure of the model, CrachFEM introduces a refinement to the initial imperfection geometry and uses isotropic-kinematic hardening for nonlinear strain paths.

Fracture criteria in CrachFEM failure model follow the generic structure of the fracture criteria in the literature. For strictly linear strain paths, a strain based damage indicator, $R$, can be expressed as follows

$$R = \frac{\varepsilon^p}{\varepsilon_f^p} \tag{1}$$

where $\varepsilon^p$ is the equivalent plastic strain and $\varepsilon_f^p$ is the equivalent plastic strain at fracture. It is not hard to guess that failure occurs when $R$ approaches unity. For the case of nonlinear strain paths, a Kolmogorov type integral formulation is more appropriate, which reads

$$R = \int_0^{\varepsilon_f^p} \frac{d\varepsilon^p}{\varepsilon_{eq}^f} \tag{2}$$

where $\varepsilon_{eq}^f$ is a path dependent function of stress state. For more complicated strain paths which comprise load reversals, CrachFEM applies a slightly more involved formulation which is not included for the sake of simplicity; see, e.g. [Dell et al., 2008] for more details.

Two fracture criteria in CrachFEM are distinguished with the definition of $\varepsilon_{eq}^f$. For the normal fracture and shear fracture, one defines two different fracture strains, $\varepsilon_{eq}^{f,normal}$ and $\varepsilon_{eq}^{f,shear}$ respectively,

$$\left.\begin{aligned} \varepsilon_{eq}^{f,normal} &= d\exp[q\beta], \\ \varepsilon_{eq}^{f,shear} &= \frac{\varepsilon_{SF}^{+}\sinh\left[f\left(\theta-\theta^{-}\right)\right]+\varepsilon_{SF}^{-}\sinh\left[f\left(\theta^{+}-\theta\right)\right]}{\sinh\left[f\left(\theta^{+}-\theta^{-}\right)\right]}. \end{aligned}\right\} \tag{3}$$

For the normal fracture strain, $d$ and $q$ denote material parameters whereas $\beta$ is the stress state dependent parameter which reads

$$\beta = \frac{1-3\eta\, s_{NF}}{\sigma_1/\sigma_{eq}^{vM}} \quad \text{with} \quad \eta = \frac{\sigma_1+\sigma_2+\sigma_3}{3\sigma_{eq}^{vM}} \tag{4}$$

where $s_{NF}$ and $\sigma_i$, $i=1,2,3$ denote a material parameter and principal components of the Cauchy stress tensor, respectively. $\sigma_{eq}^{vM}$ represents von Mises equivalent stress. Stress triaxiality ratio is denoted by $\eta$.

Coming to the shear fracture strain, $\theta$ denotes the shear stress state parameter with

$$\theta = \frac{1-3\eta\, k_{SF}}{\tau_{\max}/\sigma_{eq}^{vM}} \quad \text{with} \quad \tau_{\max} = \frac{1}{2}\left|\max(\sigma_1,\sigma_2,\sigma_3)-\min(\sigma_1,\sigma_2,\sigma_3)\right| \tag{5}$$

$\theta^{+}=2-4k_{SF}$ and $\theta^{-}=2+4k_{SF}$ denote shear stress parameter at equibiaxial tension and compression, respectively. Other determined parameters are $k_{SF}$, $f$, $\varepsilon_{SF}^{+}$ and $\varepsilon_{SF}^{-}$ where $\varepsilon_{SF}^{+}$ and $\varepsilon_{SF}^{-}$ are fracture strain values at equibiaxial tension and compression, respectively.

Figure 1 illustrates some common states of stress on a von Mises type yield locus represented in (principal) plane stress space. The states A, B, C, D and E respectively represent cases involving equibiaxial tension, plane strain, uniaxial tension, pure shear and uniaxial compression.

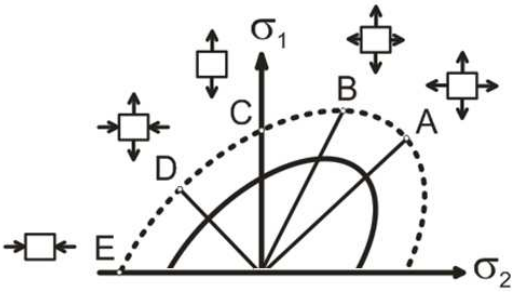


Figure 1: Stress states in plane stress conditions. A: Equibiaxial tension, B: Plane strain, C: Uniaxial tension, D: Pure Shear, E: Uniaxial compression.

A useful study will be defining mentioned stress dependent parameters for the mentioned plane stress states observed in sheet metal forming. Table 1 summarizes the parameters equivalent von Mises stress, triaxiality ratio $\eta$, and CrachFEM normal and shear fracture parameters, i.e. $\beta$ and $\theta$ for the stress states A to E. Note that, all other parameters, except for CrachFEM normal fracture and shear fracture parameters, are independent of the selected material and whereas $\beta$ and $\theta$ have a dependency through parameters $s_{NF}$ and $k_{SF}$, respectively. Accordingly, the tabulated values belog to one of the utilized materials (namely M1 as explained in Section 3.1).

Table 1: Corresponding definitions for certain stress states.

| | **Stress State** | $\sigma_1, \sigma_2$ | $\sigma_{eq}^{vM}$ | $\eta$ | $\beta$ | $\theta$ |
|---|---|---|---|---|---|---|
| A | Equibiaxial tension | $\sigma_1 = \sigma_2$ | $\sigma_1$ | $2/3$ | 0.728 | 1.864 |
| B | Plane strain tension | $\sigma_1 = 2\sigma_2$ | $\sqrt{3}\sigma_1/2$ | $\sqrt{3}/3$ | 0.662 | 1.630 |
| C | Uniaxial tension | $\sigma_1 > 0,\ \sigma_2 = 0$ | $\sigma_1$ | $1/3$ | 0.864 | 1.932 |
| D | Pure Shear | $\sigma_1 = -\sigma_2$ | $\sqrt{3}\sigma_1$ | 0 | 1.732 | 3.464 |
| E | Uniaxial Compression | $\sigma_1 = 0,\ \sigma_2 < 0$ | $\lvert\sigma_2\rvert$ | –1/3 | NA | 2.068 |

Although the exponential dependence of the normal fracture strain on the normal fracture parameter, $\beta$, is obvious, the dependence of the normal fracture and especially shear fracture strains on the triaxiality ratio is not straightforward, specifically due to the relatively complicated nature of the functional declarations. For this purpose, the shear and normal fracture strain curves are plotted in the triaxiality ratio space in Figure 2 for M1.

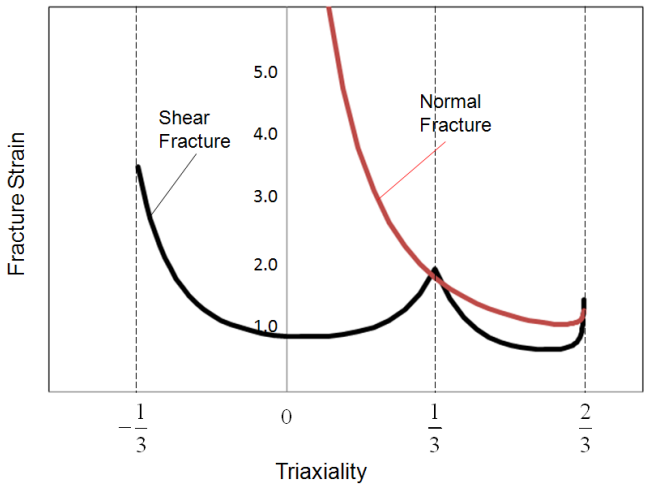


Figure 2: Shear and normal fracture strain values with respect to triaxiality ratio.

In accordance with the observations given in [Bao and Wierzbicki, 2004], the shear fracture strains in the low and negative triaxialities __that is for the triaxiality range of [-1/3, 1/3] __ drastically differ from the normal fracture strains, where a shear governing fracture mode is due. For the selected material M1, the curves also show that even for moderate high triaxiality intervals [1/3, 2/3] the mode of fracture is shear dominated.

## 3. Deep Drawing of Advanced High Strength Steel Sheets

### 3.1 Experimental Set Up

Deep drawing process with rectangular punch and die is selected as a case study due to various stress states captured at a single test. Two advanced high strength steel types, namely material 1 (M1) and material 2 (M2), produced by ThyssenKrupp Steel Europe AG are used. Geometry of the problem is denoted in Figure 3. A

constant blankholder force is applied during tests. The square punch section has an edge of 70 mm and corner fillets with radius of 10 mm. For the remaining edges 7 mm fillets are applied. Corresponding die fillets are 5 mm. The die section matches with that of the punch with a clearance of 1.05 mm for M1 and 1.55 mm for M2.

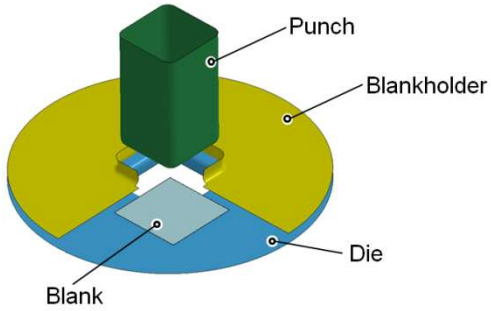


Figure 3: Schematic representation of the square cup drawing.

Square blanks with 150 mm edge lengths are used. The sheet thicknesses for M1 and M2 are 1 mm and 1.5 mm, respectively. The sheets are drawn with 0° (parallel) and 45° (diagonal) orientations with respect to the punch as indicated in Figure 4. Since the materials of interest, M1 and M2, show anisotropic characteristics, the effect of the rolling direction with respect to the blank orientation on the formability is also investigated. For this purpose, the square blanks are cut in two types of blanks with respect to rolling direction for each material. Those are parallel and diagonal rolling directions as shown in Figure 5.

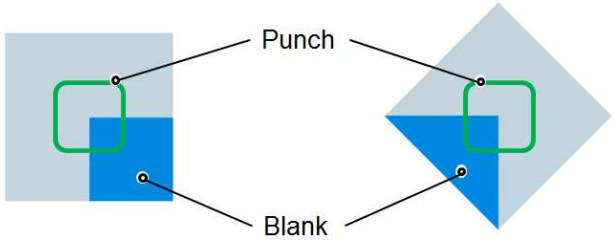


Figure 4: Applied blank orientations in the tests, (a) Parallel, (b) Diagonal.

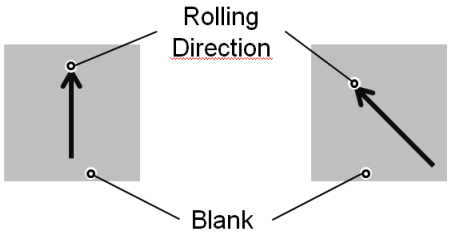


Figure 5: Applied rolling directions in the tests. (a) Parallel, (b) Diagonal.

Finally, an additional alteration is applied by conduction of experiments under different blank-holder forces where the specimens with different blank orientations and rolling directions are drawn until failure occurrence. Punch force and travel as well as the drawing depth at failure are recorded. Selected experimental cases for validation studies are tabulated in Table 2.

Table 2: Selected Experiment Specimens

| # | Material | Blank Orientation | Rolling Direction | Blank-holder Force (kN) |
|---|---|---|---|---|
| 1 | M1 | Parallel | Diagonal | 200 |
| 2 | M1 | Diagonal | Parallel | 100 |
| 3 | M1 | Diagonal | Diagonal | 120 |
| 4 | M2 | Parallel | Parallel | 50 |
| 5 | M2 | Diagonal | Parallel | 50 |
| 6 | M2 | Diagonal | Parallel | 150 |
| 7 | M2 | Diagonal | Diagonal | 50 |

For each experimental specimen, location of gridded surface for strain analysis and lubrication conditions alters which result in different friction conditions. Therefore, for each case, (Coulomb) friction coefficient is determined by means of an inverse analysis devising the punch forces.

## 3.2 Anisotropic Plasticity and Regarding Parameters

The finite element model is prepared in accordance with the problem geometry given in Figure 3 and simulations are conducted with LS DYNA which materializes CrachFEM failure model. The punch, die and blank-holder are modeled as rigid bodies. Due to symmetry conditions only a quarter geometry of the blank is modeled with 0.3 mm x 0.3 mm shell elements. To cover bending effects five integration points through thickness are used. A non-constant velocity controlled punch travel is assigned to cover a 30 mm of drawing depth. A time step of 3.7 $10^{-7}$s is selected.

In modeling of material behavior, the generic form of the yield function, which excludes kinematic hardening effects, can be given as follows

$$f\left[\underline{\underline{\sigma}}, q\right] = \sigma_{eq}\left[\underline{\underline{\sigma}}\right] - \left(\sigma_{10} + q\right) \le 0 \tag{6}$$

where $\underline{\underline{\sigma}}$ is the Cauchy stress tensor, $\sigma_{10}$ is the initial yield stress in the rolling direction and $q$ represents the yield surface expansion in stress space with isotropic hardening. Based on this generic definition it is possible to postulate different isotoropic/anisotropic and quadratic/nonquadratic yield functions just by modifying the equivalent stress definition, i.e. $\sigma_{eq}$.

Quadratic Hill 1948 yield functions are employed as alternative approaches in modeling sheet anisotropy due to rolling process. For comparison reasons, von Mises yield function which possesses isotropic plastic behavior is also utilized.

For the plane stress state, letting $\sigma_x$, $\sigma_y$ and $\sigma_{xy}$ denote the nonzero stress components, the equivalent von Mises stress, $\sigma_{eq}^{vM}$, reads,

$$\sigma_{eq}^{vM} = \sqrt{\frac{1}{2}\left(\left(\sigma_x - \sigma_y\right)^2 + \sigma_x{}^2 + \sigma_y{}^2 + 6\sigma_{xy}{}^2\right)} \tag{7}$$

Coming to quadratic anisotropic Hill 1948 type equivalent stress, $\sigma_{eq}^{Hill}$, see e.g. [Hill, 1948], one has

$$\sigma_{eq}^{Hill} = \sqrt{\frac{3}{2}\left(\left(1-a_x\right)\sigma_x{}^2 + \left(1-a_y\right)\sigma_y{}^2 - 2a_z\sigma_x\sigma_y + 2a_{xy}\sigma_{xy}{}^2\right)} \tag{8}$$

where $a_x$, $a_y$, $a_z$ and $a_{xy}$ can be defined in terms of Lankford's coefficients, i.e. $r_0$, $r_{45}$ and $r_{90}$, as follows

$$a_x = \frac{r_0}{r_0 + r_{90} + r_0 r_{90}},\ a_y = \frac{r_{90}}{r_0 + r_{90} + r_0 r_{90}},\ a_{xy} = \left(a_x + a_y\right)\left(\frac{1}{2} + r_{45}\right),\ a_z = 1 - a_x - a_y. \tag{9}$$

Purely isotropic hardening material models are insufficient for material classes which show path dependent hardening and Bauschinger effect. For such cases kinematic hardening models are proposed. Within the current treatment, in order to model kinematic hardening, without loss of generality the Cauchy stress is replaced by a relative stress, $\underline{\underline{\tau}} = \underline{\underline{\sigma}} - \underline{\underline{\beta}}$, where $\underline{\underline{\beta}}$ denotes the back stress, i.e. the translation of the yield locus,

$$f\left[\underline{\underline{\sigma}}, \underline{\underline{\beta}}, q\right] = \sigma_{eq}\left[\underline{\underline{\tau}}\right] - \left(\sigma_{10} + q\right) \le 0 \tag{10}$$

Flow curves for materials M1 and M2 are given in Figure 6 whereas the Lankford's coefficients are listed in Table 3.

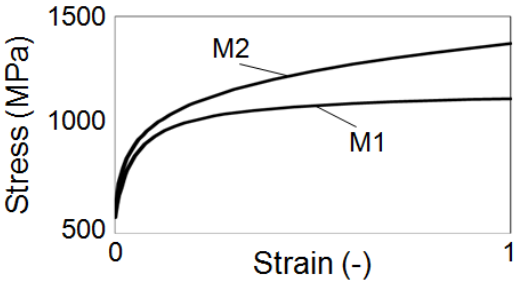


Figure 6: Strain hardening curves for M1 and M2.

Table 3: The Lankford's coefficients.

| Lankford's Coefficients | Material 1 | Material 2 |
|---|---|---|
| $r_0$ | 0.5635 | 0.5010 |
| $r_{45}$ | 0.9726 | 1.1880 |
| $r_{90}$ | 0.6686 | 0.6560 |

## 3.3 Numerical Investigations

Below we present simulation results based on the given process geometry and material parameters for M1. These simulations aim to investigate the effect of the model parameters such as orientation of blank with respect to punch, rolling definition for blank on normal and shear damage indicator distributions. These distributions are shown at the drawing depth of 15 mm, which constitutes the minimum drawing depth at which failure occurs due to instability for the given cases.

### 3.3.1 Effect of blank orientation

In order to solely study the effect of blank orientation, the effects of anisotropy with rolling process are eliminated by selection of an isotropic von Mises yield locus. As seen in the ductile normal fracture risk distributions given in Figure 7, the critical elements that have the highest risk values for both cases are placed at the same region, which is the corner of the punch.

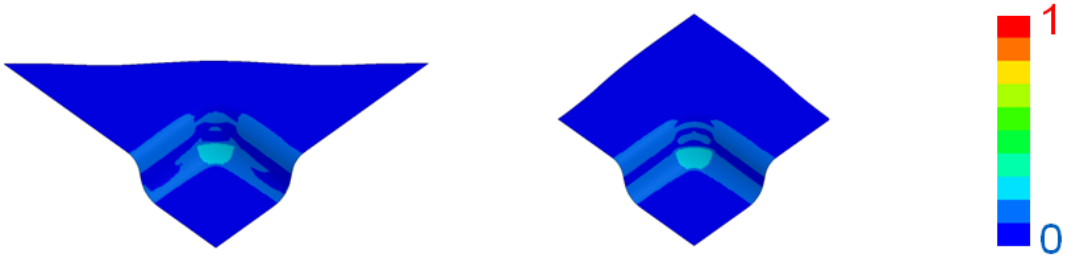


(a) (b)

Figure 7: Ductile normal fracture risk distributions for different blank orientations, (a) Diagonal, (b) Parallel.

For the shear fracture risk distributions, the observations differ. The highest shear fracture risk changes with the change of the blank orientation with respect to the punch as shown in Figure 8. However, the locations of the elements with highest shear failure risk are same for each orientation.

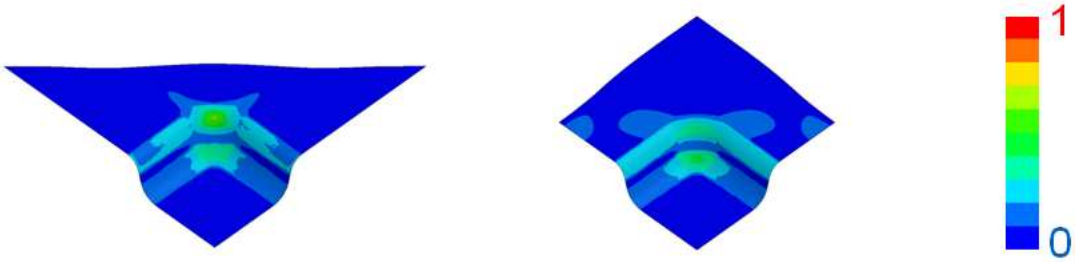


(a) (b)

Figure 8: Ductile shear fracture risk distributions for different blank orientations, (a) Diagonal, (b) Parallel.

A detailed analysis of the given cases can be seen in Figure 9.a and b where (normalized) path plots are supplied for the ductile normal and shear fracture risk values. The shift in the risk trends is noticeable especially for the shear fracture risk curves. A final remark is that, for both blank orientations the shear and normal fracture risk values are far below the critical threshold which is unity.

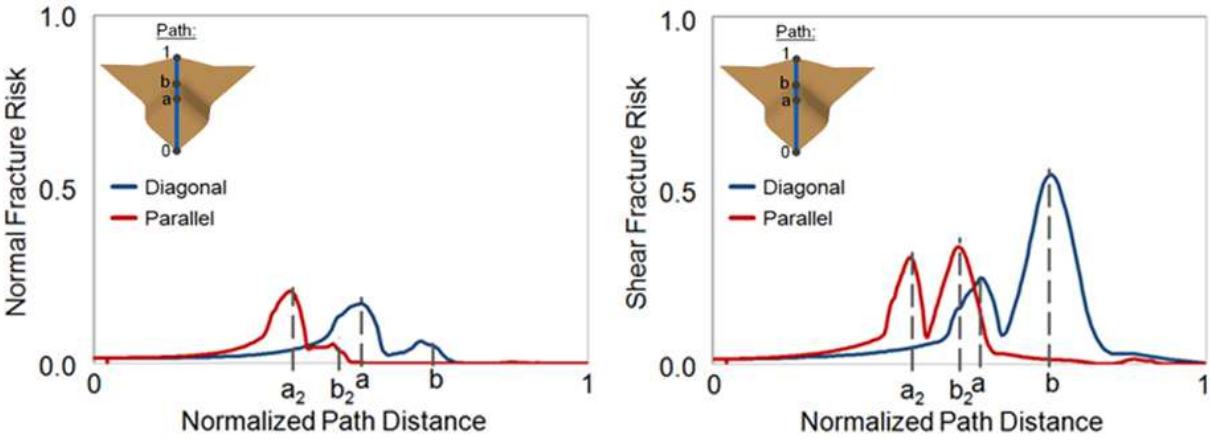


(a) (b)

Figure 9: Fracture risk values for different blank orientations, (a) Normal fracture, (b) Shear fracture.

### 3.3.2 Effect of Rolling Direction

The effect of the rolling direction on damage accumulation is studied using Hill 1948 yield function. For the so-called parallel direction, there is a noticeable increase in risk values for normal fracture as illustrated in Figure 10. As before, the critical elements that have the highest risk values for both cases are placed at the same region, which is the corner of the punch.

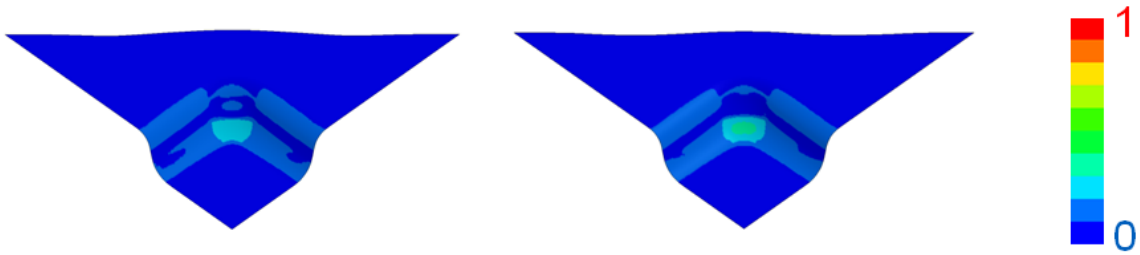


(a) (b)

Figure 10: Ductile normal fracture risk distributions for different rolling directions, (a) Parallel, (b) Diagonal.

The shear fracture risk contours are given in Figure 11. In both rolling directions, the critical accumulations do not change location. It is seen that for the diagonal rolling direction, the shear fracture risk values on the side walls are increased which are of out of plane type.

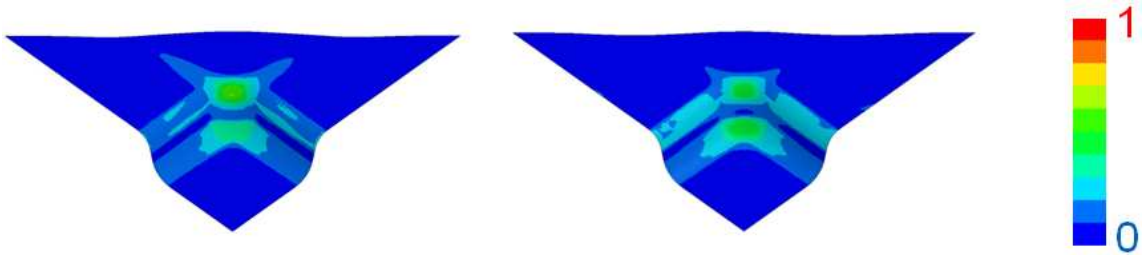


(a) (b)

Figure 11: Ductile shear fracture risk distributions for different rolling directions, (a) Parallel, (b) Diagonal.

A detailed analysis of the given cases can be seen in Figure 12.a and b where (normalized) path plots are supplied for the ductile normal and shear fracture risk values. The trends of the curves follow each other qualitatively for the normal fracture risk where at the punch corner; there occurs an increase for the diagonal direction as also noted in the contour plots. For the shear fracture risks, changing the material orientation from

diagonal to parallel increases the risk at the punch corner region whereas it decreases the risk in drawing region. In accordance with the previous analysis realized for the blank orientation effect on damage, for both rolling directions the shear and normal fracture risk values are far below the critical threshold which is unity.

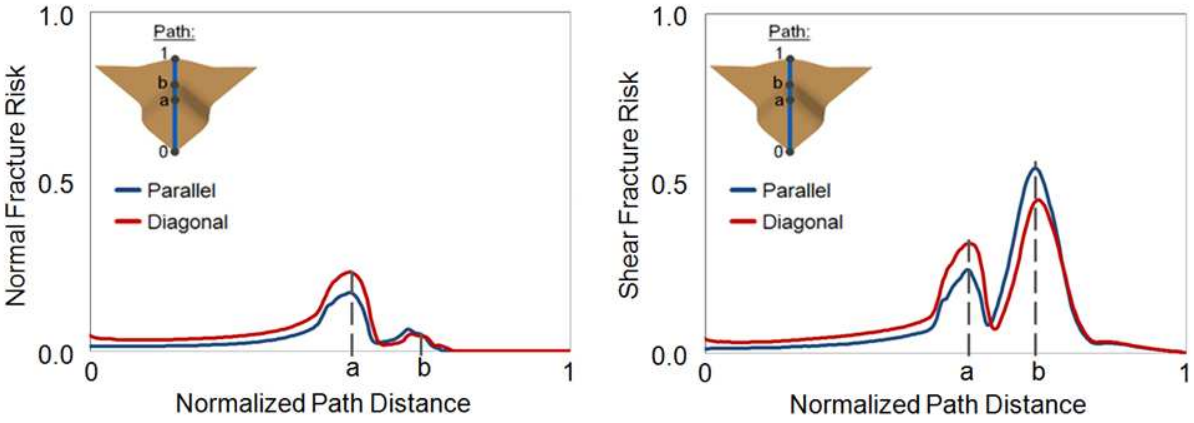


(a) (b)

Figure 12: Fracture risk values for different rolling directions, (a) Normal fracture, (a) Shear fracture.

## 3.4 Comparison of Experimental and Numerical Investigations

The numerical analysis reveal that shear and normal fracture is not critical in the selected material and process combination where the failure is due to the instability risk. By using element elimination feature of LS-DYNA, the elements whose risk values are higher than the critical threshold value are eliminated from the computational stack. As a result, the crack pattern can be simulated. Figures 13 and 14 show crack patterns obtained in the experiments and simulations for two different specimens.

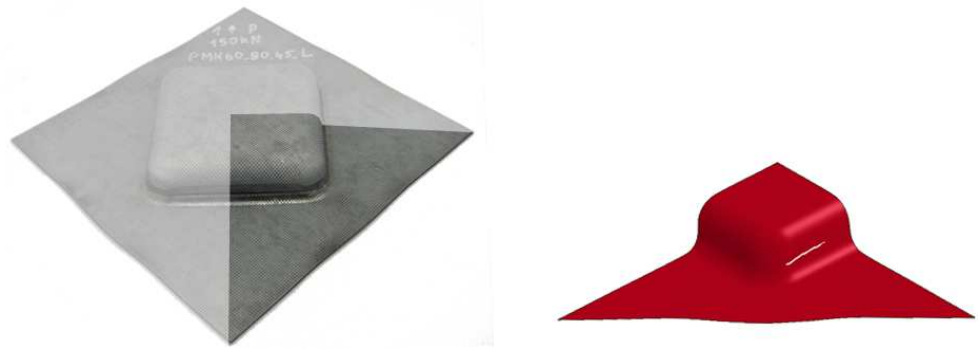

(a) (b)

Figure 13: Fracture region for specimen 6 and simulation model, (a) Experiment, (b) Simulation.

In Figure 13, the predictions of the simulations are matching with the experiments in terms of not only the failure region, but also the drawing depth at the failure. However, for several cases the predictions of the simulations deviate from the experimental outputs as seen in the Figure 14.

(a) (b)

Figure 14: Fracture region for specimen 2 and simulation model, (a) Experiment, (b) Simulation.

Figure 15 shows common fracture zones observed in the experiments.

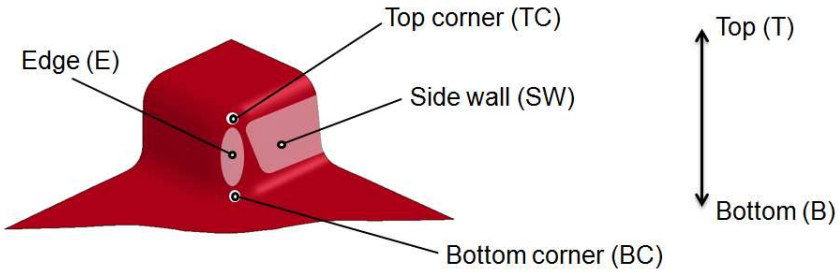


Figure 15: Naming convention used in the definition of the common failure regions.

With reference to the notation given in Figure 15, a summary of numerical and experimental failure outputs are comparison between numerical investigations and experimental results can be tabulated as follows:

Table 4: Summary of the experimental and numerical results.

| # | Material | Blank Orientation | Rolling Direction | Case | Drawing Depth at Failure (mm) | Location of Failure |
|---|---|---|---|---|---|---|
| 1 | M1 | Parallel | Diagonal | Exp. | 19 | TC |
| | | | | Sim. | 15 | Middle of the E |
| 2 | M1 | Diagonal | Parallel | Exp. | 23 | TC & SW |
| | | | | Sim. | 15 | On E & SW (closer to BC) |
| 3 | M1 | Diagonal | Diagonal | Exp. | 16 | SW (closer to B) |
| | | | | Sim. | 15 | SW (closer to B) |
| 4 | M2 | Parallel | Parallel | Exp. | 33 | TC |
| | | | | Sim. | 20 | Middle of the E |
| 5 | M2 | Diagonal | Parallel | Exp. | 19 | TC & SW |
| | | | | Sim. | 22 | BC & SW |
| 6 | M2 | Diagonal | Parallel | Exp. | 16 | SW (closer to B) |
| | | | | Sim. | 16 | SW (closer to B) |
| 7 | M2 | Diagonal | Diagonal | Exp. | 16 | SW (closer to B) |
| | | | | Sim. | 20 | BC & SW (closer to B) |

When the comparisons are examined, two specimens, namely specimen 3 and specimen 6, have promising predictions on the failure drawing depth and its location. However, for specimen 2 and specimen 4, neither failure drawing depth nor its location is correctly predicted. For these cases, an instability type failure is experimentally captured with thinning observed at the fractured edges. For a better understanding, we use the representation of the initial FLCs in strain rate ratio equivalent plastic strain space following [Müschenborn and Sonne, 1975], where the strain state parameter, $\alpha$ is defined as

$$\alpha = \frac{\dot{\varepsilon}_2}{\dot{\varepsilon}_1} \tag{11}$$

CrachFEM uses a transiently updated FLC which depends on the strain path. Figure 16 shows the strain path plot of the (instability) critical elements with respect to the initial FLC for M1. As observed, for accurate predictions, i.e. specimen 3 and 6, the strain paths passes through the instability region by cutting the curve. Since the FLC that CrachFEM utilizes considers only tensile instability, it is not defined for $\alpha < -0.5$. Accordingly, for deformation paths with an initial linear part taking place at $\alpha < -0.5$ up to larger equivalent plastic strains followed by a change towards $\alpha > -0.5$ the predicted instability failure strain is too conservative, as in the case of specimens 2 and 4, which is not in accordance with the experimental outputs.

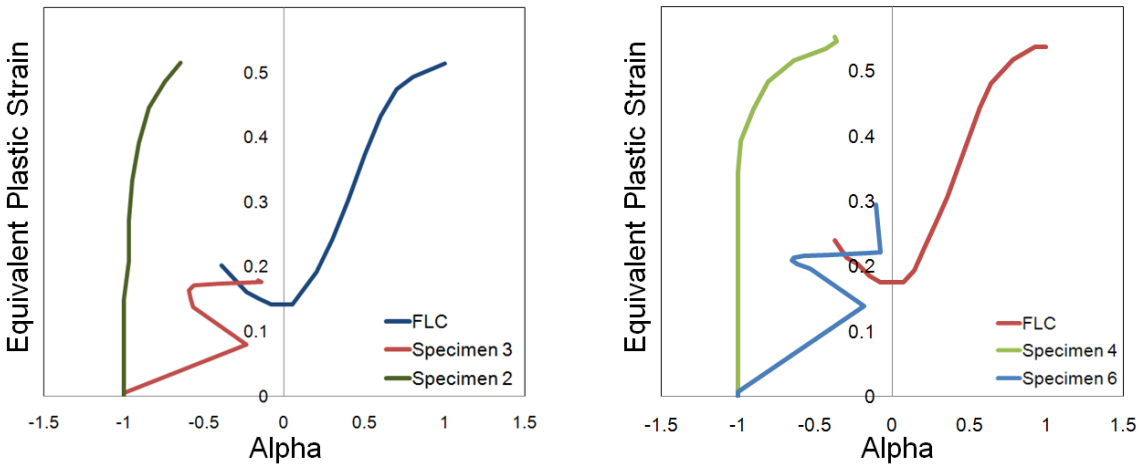


(a) (b)

Figure 16: Strain paths for most critical element with respect to instability for two specimen cases in comparison with the initial FLC, (a) M1, (b) M2.

## 4. Conclusions

We have presented formability analysis of two CP steel grades, with both experimental and numerical aspects. The experimental studies involve rectangular deep drawing tests conducted in the facilities of ThyssenKrupp Steel Europe AG. The tests are run for different blank orientations with respect to the punch and different rolling directions with respect to the blank edge and different blank-holder pressures. It is shown that, for the selected materials and the loading cases, the formability is almost always limited by instability accompanied by necking whereas in plane shear fracture does not appear in the drawing zone.

Numerical studies, conducted using LS-DYNA and material model MF GenYld+CrachFEM, show that formability assessments of CrachFEM are in general in correlation with the experimental outputs. The model plausibly reflects the effects of anisotropy and blank orientation on the material deterioration. However, there is still room for model improvement especially for the loading paths involving an initial deformation in shear up to relatively high equivalent strains followed by a change of the loading towards plane strain tension.

## 5. Acknowledgements

The first author, K.I., gratefully acknowledges the financial support of ThyssenKrupp Steel Europe AG. The authors also gratefully acknowledge the fruitful discussions with Dr. Gese (of MATFEM) and collaboration of MATFEM in this project with supplying free license for material model MF GenYld+CrachFEM.

## References

Bao, Y., Wierzbicki, T., 2004: “On fracture locus in the equivalent strain and stress triaxiality space”, Int. J. of Fracture, 161, 1.
Dell, H., Gese, H., Oberhofer, G., 2008: Users’ manual MF GenYld + CrachFEM 3.8: Theory.
Hill, R., 1948: “A theory of the yielding and plastic flow of anisotropic metals”, Proc. R. Soc. Lond. A193, 281.
Hosford, W.F. and Caddell, R.M., 1993: Metal Forming - Mechanics and Metallurgy, 2nd edn. Englewood Cliffs, NJ: Prentice-Hall.
Li, Y., Luo, M., Gerlach, J., Wierzbicki, T., 2010: “Prediction of shear-induced fracture in sheet metal forming”, Journal of Materials Processing Technology, 210, 1858.
Marciniak, Z. and Kuczynski, K., 1967: “Limit strains in the processes of stretch-forming sheet metal”, Int. J. Mech. Sci., 9, 609.
Müschenborn, W. and Sonne, H. M., 1975: “Einfluß des Formänderungswegesauf die Grenzformänderung von Feinblechen (Influence oft he strain path on the forming limits of sheet metal)”, Arch. Eisenhüttenwesen 46, 9, 597.